Research Article | Vol. 10, No. 2 | 1 Feb 2019 | BIOMEDICAL OPTICS EXPRESS 879
Biomedical Optics EXPRESS

Smartphone-based multispectral imaging and machine-learning based analysis for discrimination between seborrheic dermatitis and psoriasis on the scalp

SEWOONG KIM,[1] JIHUN KIM,[1] MINJOO HWANG,[1] MANJAE KIM,[1] SEONG JIN JO,[3] MINKYU JE,[2] JAE EUN JANG,[1] DONG HUN LEE,[3,4] AND JAE YOUN HWANG[1,5]

[1]*Department of Information and Communication Engineering, Daegu Gyeongbuk Institute of Science & Technology, Daegu, 42988, South Korea*
[2]*School of Electrical Engineering, Korea Advanced Institute of Science and Technology, Daejeon, 34141, South Korea*
[3]*Department of Dermatology, Seoul National University College of Medicine, Institute of Human-Environment Interface Biology, Seoul National University, Seoul, 03080, South Korea*
[4]*ivymed27@snu.ac.kr*
[5]*jyhwang@dgist.ac.kr*

Abstract: For appropriate treatment, accurate discrimination between seborrheic dermatitis and psoriasis in a timely manner is crucial to avoid complications. However, when they occur on the scalp, differential diagnosis can be challenging using conventional dermascopes. Thus, we employed smartphone-based multispectral imaging and analysis to discriminate between them with high accuracy. A smartphone-based multispectral imaging system, suited for scalp disease diagnosis, was redesigned. We compared the outcomes obtained using machine learning-based and conventional spectral classification methods to achieve better discrimination. The results demonstrated that smartphone-based multispectral imaging and analysis has great potential for discriminating between these diseases.

1. Introduction

Seborrheic dermatitis and psoriasis are common chronic inflammatory skin diseases that present with erythematous scaly skin lesions. Approximately 3% of individuals worldwide currently experience these diseases, and more than 3 million individuals are treated in the USA and United Kingdom each year. Seborrheic dermatitis typically occurs on the scalp or the face, usually manifesting as oily and greasy inflammation. Its symptoms include itching, reddish skin, and flaking on greasy skin areas [1]. Conversely, psoriasis, which is now considered as a multifactorial immune-mediated disease, is manifested by itching, reddish skin, and silvery-white scaly plaques on the scalp, face, or extremities [2,3].

Although neither seborrheic dermatitis nor psoriasis is fatal to humans, both diseases are associated with significant physical and psychological burden. Accurate/preemptive diagnosis of these diseases is thereby crucial to control their symptoms and predict their prognosis, in terms of their chronic and relapsing properties and associated comorbidities, such as metabolic syndrome [4,5]. For this purpose, an advanced tool capable of diagnosing the diseases at home, a local hospital, or elsewhere with high accuracy would be beneficial for better treatment and management. However, using a conventional dermascope, the discrimination between seborrheic dermatitis and psoriasis has been clinicopathologically very challenging. In particular, when these diseases occur only on the scalp, the differential diagnosis between them is more challenging even among experienced physicians owing to their similar features [6,7].

#353125 https://doi.org/10.1364/BOE.10.000879
Journal © 2019 Received 28 Nov 2018; revised 11 Jan 2019; accepted 11 Jan 2019; published 24 Jan 2019

Biomedical Optics EXPRESS

Recently, dermatologists have been exploring new methods for better diagnosis of seborrheic dermatitis and psoriasis. Among them, a videocapillaroscope, which provides high magnification, has been used to examine and classify the morphological shape of the capillaries to distinguish the diseases accurately [8,9]. However, the shape of the capillaries is immensely sensitive to external environments, and as a result, the outcomes have been shown to vary [10]. Moreover, the diagnosis using the device can be only realized by dermatologists in a hospital. Thus, it may not be suited for preemptive diagnosis of the diseases under ubiquitous environments. Therefore, development of more advanced tools is needed for better mobile diagnosis of seborrheic dermatitis and psoriasis on the scalp.

Spectral imaging and analysis techniques have been widely used for the non-invasive diagnosis of diseases occurring on the skin and scalp [11,12]. In particular, they offer high sensitivity and specificity in the detection of various diseases, which is not possible using monochrome and RGB color [13–16]. For this reason, spectral imaging and analysis may also be applicable in discriminating between seborrheic dermatitis and psoriasis on the scalp with high accuracy, since it can differentiate slight spectral differences between diseases with different biological compositions. However, conventional spectral imaging systems are relatively bulky; thus, they need to be miniaturized and combined with information technology (IT) for self-diagnosis of these diseases. Therefore, for the expedient self-diagnosis of seborrheic dermatitis and psoriasis on the scalp, a new type of multispectral imaging system based on IT as well as a relevant spectral analysis technique is needed.

Thus, we built a smartphone-based multispectral imaging system for scalp care and investigated the potential of various multispectral imaging and analysis methods to discriminate between seborrheic dermatitis and psoriasis on the scalp using the system. The smartphone-based multispectral imaging system consisted of an external CMOS camera and a light-emitting diode (LED) array, including narrow bandpass filters. The system was connected to a smartphone for image acquisition, image transfer, and image analysis in a server and classified image display [17]. After evaluating the performance of the system, it was employed to discriminate between seborrheic dermatitis and psoriasis on the scalp of patients. Moreover, to achieve a more accurate diagnosis of the diseases, various machine learning-based and conventional spectral imaging and analysis techniques were applied for spectral classification, and their outcomes were compared.

2. Methods

We built a smartphone-based multispectral imaging system with an external CMOS camera for the diagnosis of seborrheic dermatitis and psoriasis on the scalp. This system consisted of a multispectral imaging module, which included an LED array, various optical components, a CMOS camera (See3CAMCU50, E-CON SYSTEMS) connected to the smartphone, and an interface circuit for synchronization between the CMOS camera and the LED array, and a system control/image analysis module, which included a smartphone (SM-G935, SAMSUNG) and a server [Fig. 1(a)].

The LED array included nine white LEDs (Iws-351-white, ITSWELL). Eight of the LEDs were utilized for multispectral imaging, and one LED was utilized to examine the regions of interest. After a linear variable filter (LF102499, DELTA OPTICS) was diced to construct narrow bandpass filters, each diced linear variable filter was placed prior to each LED to select the wavelengths of the light emitted from the LED. The sizes of the diced filters were measured to be 3.8 mm (width) × 3.3 mm (height) × 2.5 mm (thickness). The center wavelengths of the filters were ~453 nm (FWHM: 9.3 nm), ~493 nm (FWHM: 11 nm), ~520 nm (FWHM: 12.3 nm), ~545 nm (FWHM: 13.3 nm), ~580 nm (FWHM: 15.6 nm), ~605 nm (FWHM: 16.2 nm), ~638 nm (FWHM: 16.6 nm), and ~663 nm (FWHM: 16.8 nm) [Fig. 1(b)]. The filtered light emitted from the selected LED was illuminated onto the skin regions of interest on the scalp after passing through a polarizer oriented in the vertical direction. The reflected light from the skin passing through another polarizer, oriented in the horizontal

Biomedical Optics EXPRESS

direction, was collected using a lens (IR0618B5M, FIFO Optics) and recorded in the 5M pixel color CMOS camera. The cross-polarizers allowed scattered light to be obtained while rejecting specular reflected light from the skin [18].

In the system, an interface circuit was built to synchronize between the CMOS camera and the LED module. The circuit consisted of a microprocessor unit (ATMEGA128, Atmel), A Bluetooth low energy module (Bot-Cle 110, Chipsen), a constant current chip (MBI5026, Macroblock) for supplying constant current to the LEDs, a regulator (TPS73033, Texas Instruments), and a level shifter (NCP1402, ON Semiconductor)The microprocessor unit received command signals from the Android application via the Bluetooth module and then turned on/off an LED to select light wavelengths. A 3.7-V lithium-polymer battery was utilized to supply electric power to the interface circuit. After 3.7 V was up-regulated to 5 V, 5 V was supplied to the microprocessor unit and a constant current chip. Conversely, after 3.7 V was down-regulated to 3.3 V, it was then supplied to the Bluetooth module. The level shifter adjusted the level of data voltages to achieve reliable communication between the microprocessor unit and the Bluetooth module. Figure 1(c) illustrates the diagram of the interface circuit.

In the synchronization between the CMOS camera and the LED module, a smartphone controlled the interface circuit through the Bluetooth communication whereas the smartphone controlled the CMOS camera through the cable since the CMOS camera module did not have the Bluetooth communication functionality. When the interface circuit received a command from the smartphone through Bluetooth communication, one LED at a specific wavelength was selected, and then the interface circuit sent an acknowledgment to the smartphone. After the smartphone received the acknowledgment from the interface circuit, the smartphone sent a commend to the CMOS camera for acquisition of a skin image through the wired communication.

For multispectral imaging and analysis, images at eight different consecutive wavelengths, i.e., an image cube, were sequentially recorded in the camera after the light wavelength was selected by turning on an LED at a selected wavelength. The image cube was then transferred to a server through Wi-Fi or LTE communications for multispectral image analysis as shown previously. The multispectral analysis was performed by the constructed machine learning models in the server. The analyzed result was transferred to a smartphone and then displayed in the smartphone. The typical diagnosis time including image acquisition, image transfer, and image processing time was measured to be less than 12 seconds. Figure 1(d) illustrates the image of the system.

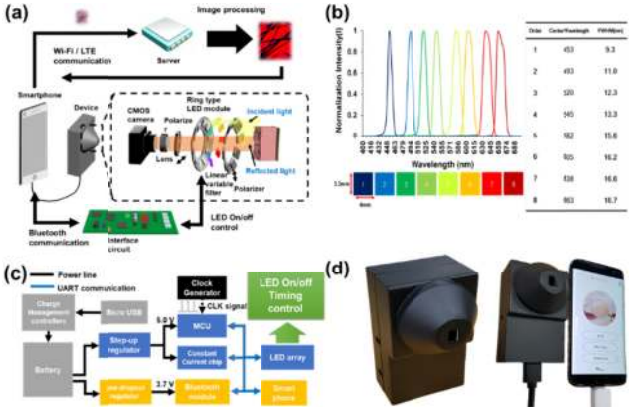

Fig. 1. Smartphone-based multispectral imaging system for the diagnosis of seborrheic dermatitis and psoriasis on the scalp: (a) diagram of the smartphone-based multispectral imaging system, (b) transmission spectra of diced variable tunable filters (size of the filters: 3.8 mm × 3.3 mm × 2.5 mm), (c) schematics of an interface circuit, and (d) image of the smartphone-based multispectral imaging system.

Biomedical Optics EXPRESS

2.1 Spectral classification using conventional linear distance measures and machine learning techniques

To discriminate between seborrheic dermatitis and psoriasis on the scalp, machine learning techniques, including the support vector machine (SVM), logistic regression (Logi), and multilayer perceptron (MLP) techniques, and conventional linear distance measurement methods, such as the Euclidean distance (ED) and spectral angle mapper (SAM), were applied for spectral classification. Before the obtained image cube was applied for spectral classification, it was preprocessed via calibration, as shown previously [19]. For spectral classification of the spectral signature of every pixel, the similarity between the spectral signatures and reference signatures, extracted from the skin lesions of interest, was calculated using the trained model based on the machine learning techniques and the distance measurement methods [20,21].

In the conventional linear distance measurement methods, the smaller the similarity values of each reference, the closer it is to the reference signatures. The similarity between the spectral signatures and reference signatures calculated using the ED and SAM can be demonstrated as the straight distance (ED) and the angle (SAM) between two vectors [Figs. 2(a) and (b)] [19]. However, their construction model procedures are quite different from the machine learning-based techniques. For spectral classification using the machine learning techniques, a training data set, which includes the ground truths in advance, was first trained using the methods to construct models suited for the classification of two reference signatures with high accuracy, unlike the traditional methods with fixed models for calculating the similarities. The spectral signature was considered to be a vector, and the similarity was calculated using an equation derived from their own function in the machine learning techniques. In the machine learning techniques, the process for constructing each machine learning model was different from each other. For example, Logi uses the sigmoid function for building an optimized model for the binary classification [Fig. 2(c)], whereas the SVM finds the best hyperplane, which can distinguish the given data set successfully with low errors [Fig. 2(d)]. Conversely, the node, known as neuron, in the MLP model receives some features from the previous nodes by multiplying its weights with the activation function, and then the final output of the transferred values is compared to the ground truths [Fig. 2(e)] [22]. The machine learning models were implemented into the server using Scikit-learn library. Here we determined the key parameters for each method to achieve the best outcome using a grid search method [23]. For the logistic regression, the inverse of regularization strength parameter was determined to be 0.0303. For the support vector machine, the kernel type was linear, and the penalty parameter C was 0.1. For the multilayer perceptron, the hidden layer size was 4, 4, 4, the activation function was ‘Identity’, the learning rate was 1.0, and the optimizer type was ‘Adam’.

For the training and testing of the machine learning models, 18000 spectral signatures obtained from the lesions of interest were utilized as the training set, while the unused 2000 spectral signatures were utilized as the test set. In addition, 10-fold cross-validation was performed to assess the generalization of the models [20]. The cross-validation technique is a conventional validation technique for quantitatively evaluating the outcomes of a trained model.

Biomedical Optics EXPRESS

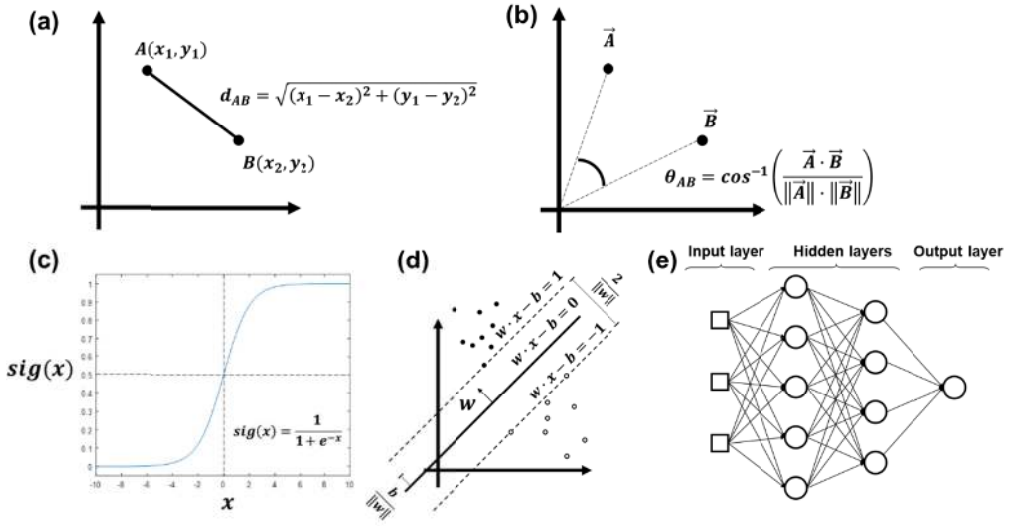

Fig. 2. Implemented spectral classification models: (a) Euclidean distance, (b) spectral angle mapper, (c) logistic regression, (d) support vector machine, and (e) multilayer perceptron.

After the classification of the images using the implemented models in the server, we removed the hair areas separated from the classified image. Thereafter, the probabilities of the spectral classified images to indicate psoriasis and seborrheic dermatitis were obtained to estimate the potential skin disease on the scalp using the following equations:

$$P_{(PS)} = \frac{number\ of\ pixels_{(PS)}}{number\ of\ pixels_{image} - number\ of\ pixels_{hair}}$$
$$P_{(PS)} > Th \rightarrow PS,\ P_{(PS)} \le Th \rightarrow SD \quad (1)$$
$$\arg\max_{Th} f(Th) := \{th \mid \forall y : f(y) \le f(th)\}$$

where PS is psoriasis; SD, seborrheic dermatitis; $P_{(PS)}$, the probability of the PS classified pixel; *Th,* the threshold value to maximize the accuracy in the discrimination between PS and SD; and *f(Th)*, the accuracy in the discrimination between PS and SD.

2.2 Clinical trial for multispectral imaging and analysis

A clinical trial was conducted at Seoul National University Hospital (SNUH) to perform multispectral imaging and analysis using the developed smartphone-based multispectral imaging system. Multispectral images of the scalp of 60 patients (number of patients with seborrheic dermatitis: 20, number of patients with psoriasis: 20, and number of patients without these diseases: 20) were obtained using the system, followed by spectral classification. The diseases of the patients were confirmed by three different medical doctors. Also, spectral signatures from each type of diseased regions, which were confirmed by the clinicians, were extracted for the machine learning training and test. The diagnosis of seborrheic dermatitis and psoriasis is typically realized via visual inspection; thus, biopsies were not performed for diagnosis. The clinical trial was approved by the Institutional Review Boards of SNUH. The trials were performed in accordance with the relevant guidelines and regulations, and informed consent was obtained from the participants.

Biomedical Optics EXPRESS

2.3 Quantitative analysis for discriminating between seborrheic dermatitis and psoriasis using multispectral imaging and analysis

For quantitative analysis, the outcomes obtained using the models constructed with spectral signatures from an image cube were compared. In particular, receiver-operating characteristic (ROC) curves and the associated areas under the curve (AUCs) of the models in the classification were obtained and compared using the Scikit-learn library [23]. In addition, the accuracy, sensitivity, and specificity of the models in the discrimination between seborrheic dermatitis and psoriasis were obtained for statistical analysis.

2.4 Evaluation of the smartphone-based multispectral imaging system

To evaluate the smartphone-based multispectral imaging system, the optical resolution of the system was measured; imaging of a resolution target (Thorlabs, R2L2S1P1) was performed to measure the highest frequency line set that could be obtained using the system. Further, the system was compared to a multispectral imaging system based on a liquid-crystal tunable filter (LCTF) for further evaluation of its performance for multispectral imaging and analysis as previously reported [19]. Figure 3 shows an image of the resolution target obtained using the system and the intensity profiles along the vertical and horizontal dotted lines at the indicated frequency line sets. In the frequency line set of 45, the lines in the vertical (A') and horizontal (B') directions were clearly distinguished using the system [Fig. 3(b)]. Therefore, these results showed that the system could resolve 45 cycles per millimeter.

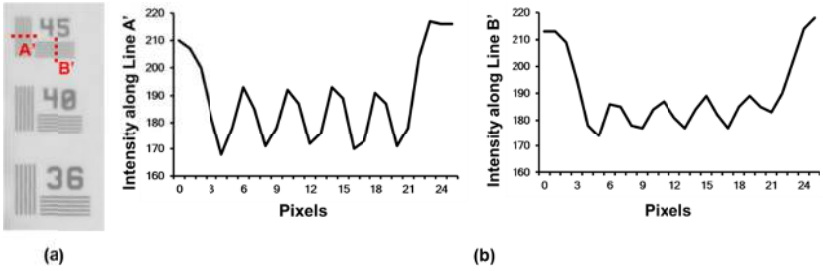

Fig. 3. Analysis of a high-frequency line set in a resolution target: (a) image of the resolution target and (b) intensity profile along the dotted line A' (left) and the dotted line B' (right).

For the LCTF-based multispectral imaging and analysis, an LCTF-based multispectral imaging system including an objective lens (Olympus, RMS4X), an LCTF (Thorlabs, KURIOS-VB1), 12 high-intensity white LEDs (ITSWELL, IWS-351), and a monochrome CMOS camera (IDS, UI-337XCP-NIR) were utilized [19]. In the LCTF-based multispectral imaging system, the light emitted from the LEDs was illuminated onto a target after passing through a polarizer in the p-direction. The light reflected from the target was collected by the objective lens and then passed through the LCTF including a polarizer in the s-direction. The filtered light was then recorded in the CMOS camera.

Figure 4 shows the spectral classified images of a target sample within the region of interest; letters "M," "B," "I," and "S" printed on a white paper in red, green, blue, and yellow, respectively, were obtained using the respective systems. In both images at the different wavelengths, letters "M" and "S" showed increased brightness as the wavelength increased, whereas letters "B" and "I" showed high brightness at 520 nm and 453 nm, respectively. Therein, the brightness variations of the letters in the image obtained using our system were in good agreement with those of the letters in the image obtained using the LCTF-based multispectral imaging system. Moreover, in the spectral classified images, the outcomes from the LCTF-based multispectral imaging system exhibited more shot noise and misclassified regions than did those from the smartphone-based imaging system. This confirmed that the smartphone-based multispectral imaging system offered slightly better outcomes than did the LCTF-based multispectral imaging system. The smartphone-based

Biomedical Optics EXPRESS

multispectral imaging system may then provide improved multispectral imaging and analysis of skin lesions on the scalp comparable to the LCTF-based multispectral imaging system.

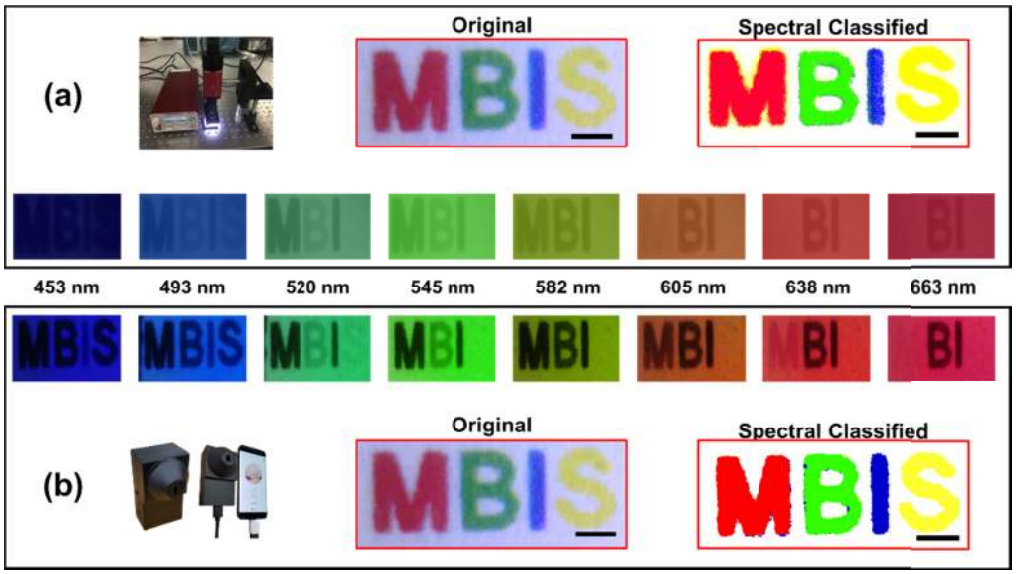

Fig. 4. Comparisons between the spectral classified images obtained using the (a) liquid-crystal tunable filter-based (field of view: 3.31 mm x 1.27 mm, pixel size: 1974 x 762, and magnification: 4x) and (b) smartphone-based multispectral imaging systems (field of view: 3.3 mm x 1.3 mm and pixel size: 760 x 276, and magnification: 4x).

3. Results

3.1 Discrimination between seborrheic dermatitis and psoriasis regions on the scalp via multispectral imaging and analysis

Clinical trials were conducted to perform multispectral imaging and analysis of seborrheic dermatitis, psoriasis, and normal regions on the scalp using the developed system. This was followed by the construction of the spectral classified images using the constructed models based on the machine learning techniques, including Logi, SVM, and MLP, and conventional linear distance measurement methods, including ED and SAM. Figure 5 illustrates the spectral classified images obtained using multispectral imaging and analysis based on the indicated techniques. The spectral images of psoriasis obtained using the ED, SAM, Logi, SVM, and MLP [Fig. 5(a), upper] exhibited red-colored regions in most of the pixels, whereas the spectral images of seborrheic dermatitis obtained using the ED, Logi, SVM, and MLP [Fig. 5(a), lower] exhibited blue-colored regions in most of the pixels. However, the spectral classified image of seborrheic dermatitis obtained using the SAM showed red-colored regions in many pixels. Therein, the red and blue colors indicated psoriasis and seborrheic dermatitis regions, respectively, while the black color indicated hair regions. These results demonstrated that the spectral classified images allowed discrimination between psoriasis and seborrheic dermatitis on the scalp. However, in the RGB images, they can hardly be distinguished. Figure 5(b) illustrates the reference spectral signatures of seborrheic dermatitis, psoriasis, and normal skin. The spectral signatures of seborrheic dermatitis and psoriasis had a peak intensity at 663 nm. They were clearly discernable at ~520 nm.

Biomedical Optics EXPRESS

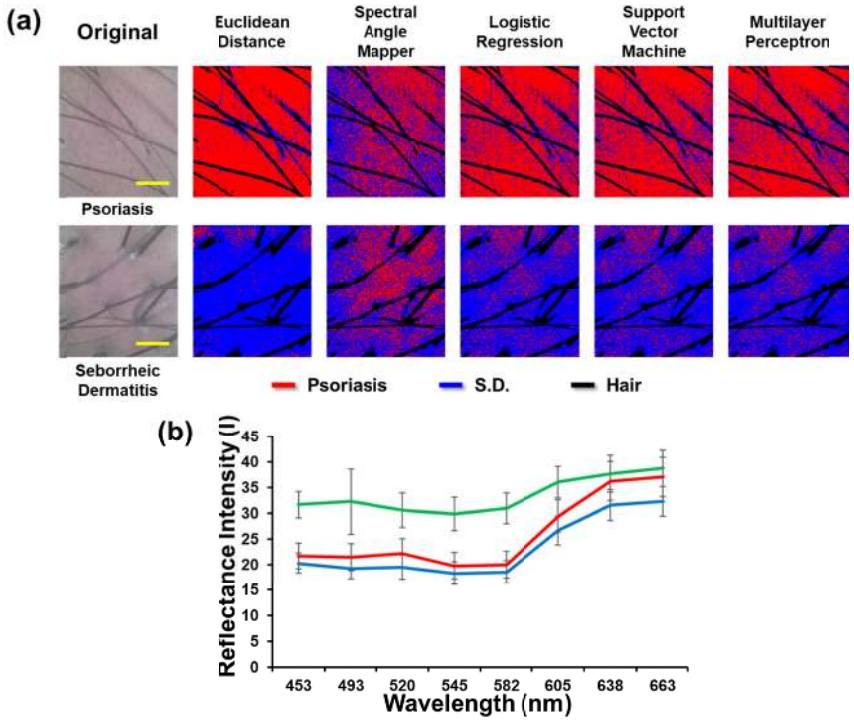

Fig. 5. Spectral classification using the traditional spectral classification methods (Euclidean distance and spectral angle mapper) and constructed models based on logistic regression, support vector machine, and multilayer perceptron: (a) photographic and classified images of psoriasis (top) and seborrheic dermatitis regions (bottom) on the scalp obtained via analysis of multispectral imaging (field of view: 3.3 mm x 2.99 mm, pixel size: 760 x 651, and magnification: 4x) and (b) reference spectral signatures of seborrheic dermatitis and psoriasis.

Table 1. Quantitative analysis of the constructed models[a]

Model	*ROC-AUC*	*Accuracy(%)*	*Sensitivity(%)*	*Specificity(%)*
ED	0.75	70	70	70
SAM	0.66	72.5	70	75
Logi	0.72	72.5	65	80
SVM	0.76	72.5	75	70
MLP	0.73	72.5	75	70

[a]using the Euclidean distance (ED), spectral angle mapper (SAM), logistic regression (Logi), support vector machine (SVM), and multilayer perceptron (MLP) with reference spectral signatures in the discrimination between seborrheic dermatitis and psoriasis on the scalp (total number of patients = 40); ROC-AUC, area under the receiver-operating characteristic curve

For the quantitative analysis of the constructed models in the discrimination between seborrheic dermatitis and psoriasis, ROC-AUCs, accuracy, sensitivity, and specificity of the models were compared. The ROC-AUCs for the ED and SAM were calculated to be 0.75 and 0.66, respectively. In contrast, the AUCs for the SVM, Logi, and MLP were 0.77, 0.72, and 0.73, respectively (Table 1). Conversely, the maximum accuracy of the models in the discrimination between the diseases was quite similar to each other. However, the SVM and MLP offered the highest sensitivity, whereas Logi offered the highest specificity. These results indicate that the machine learning-based models offered better outcomes than did the linear distance measurement models for the diagnosis of these diseases on the scalp.

Biomedical Optics EXPRESS

3.2 Discrimination between seborrheic dermatitis/psoriasis and normal regions on the scalp

Figure 6 illustrates the spectral classified images in the discrimination between psoriasis and normal skin and between seborrheic dermatitis and normal skin. The spectral classified images shown at the top of Figs. 6(a) and (b) exhibited psoriasis and seborrheic dermatitis regions in most of the pixels, whereas the spectral images shown at the bottom of Figs. 6(a) and (b) exhibited normal skin regions in a considerable number of pixels. Therein, the red, blue, and green colors represented psoriasis, seborrheic dermatitis, and normal skin regions, respectively. The spectral classified images of the patients with psoriasis showed only a few misclassified regions [Fig. 6(a), top]. Further, in the spectral classified images of the seborrheic dermatitis regions obtained using most of the models, a larger portion of the overall regions was classified as seborrheic dermatitis regions [Fig. 6(b), top]. However, in the spectral classified image obtained using the SAM, a large portion of misclassified regions was observed. In contrast, the spectral classified images of normal skin only showed a few misclassified regions [Figs. 6(a) and (b), bottom]. Therefore, these results demonstrate that the models have a good performance in the discrimination of these diseases on the scalp from the normal scalp regions.

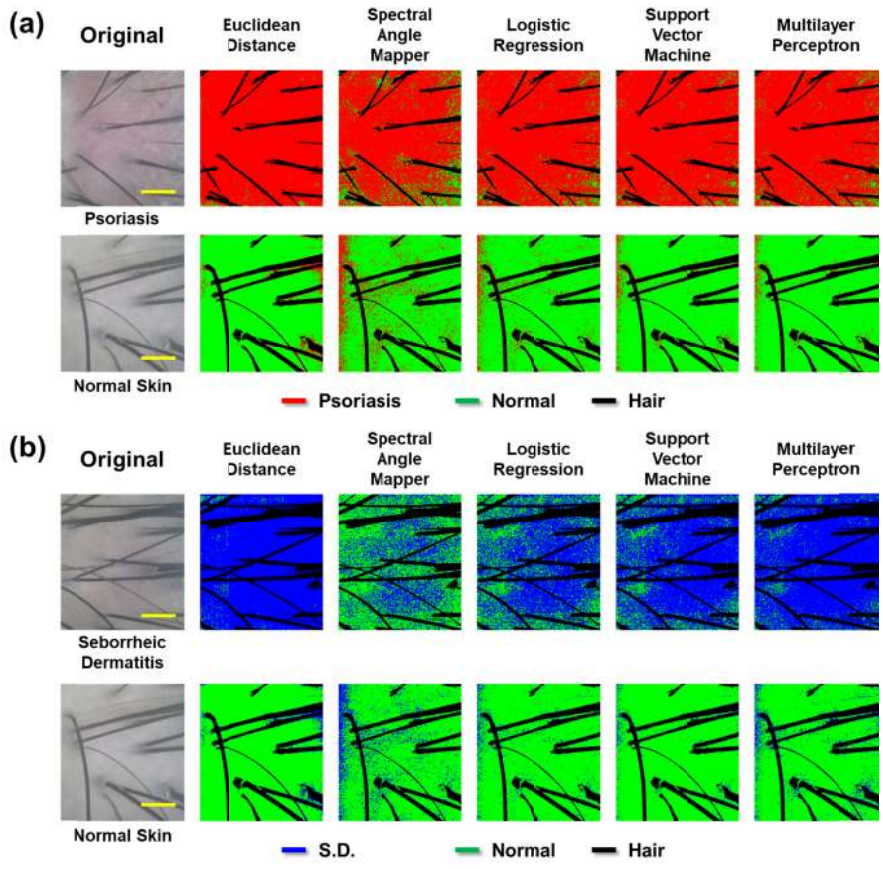

Fig. 6. Spectral classification using the constructed models: (a) photographic and classified images of psoriasis (top) and normal skin regions (bottom) and (b) photographic and classified images of seborrheic dermatitis (SD)(top) and normal skin regions (bottom) on the scalp (field of view: 3.3 mm x 2.99 mm, pixel size: 760 x 651, and magnification: 4x).

Biomedical Optics EXPRESS

For the quantitative analysis of the models, the ROC-AUC, accuracy, sensitivity, and specificity of the models were compared. All the models showed great performance in the discrimination between the diseased and normal skin regions. Among them, the SAM model yielded the best outcomes in the discrimination between the diseased and normal skin regions, unlike in the discrimination between psoriasis and seborrheic dermatitis. The ROC-AUC, accuracy, sensitivity, and specificity of the SAM model were 0.98, 95, 90, and 100 for the discrimination between psoriasis and normal skin. Further, the ROC-AUC, accuracy, sensitivity, and specificity were 1.00, 100, 100, and 100 for the discrimination between seborrheic dermatitis and normal skin (Tables 2 and 3). The ROC-AUC and accuracy of the SAM model were higher than those of the other models.

Table 2. Quantitative analysis of the constructed model for psoriasis versus normal skin[a]

Model	*ROC-AUC*	*Accuracy(%)*	*Sensitivity(%)*	*Specificity(%)*
ED	0.81	82.5	80	85
SAM	0.98	95	90	100
Logi	0.96	95	90	100
SVM	0.94	95	90	100
MLP	0.92	95	90	100

[b]using the Euclidean distance (ED), spectral angle mapper (SAM), logistic regression (Logi), support vector machine (SVM), and multilayer perceptron (MLP) with reference spectral signatures in the discrimination between psoriasis and normal skin on the scalp (total number of patients = 40, number of patients with psoriasis = 20, and number of normal subjects = 20). ROC-AUC, area under the receiver-operating characteristic curve

Table 3. Quantitative analysis of the constructed model for seborrheic dermatitis versus normal skin[c]

Model	*ROC-AUC*	*Accuracy(%)*	*Sensitivity(%)*	*Specificity(%)*
ED	0.96	90	95	85
SAM	1.00	100	100	100
Logi	0.99	97.5	95	100
SVM	0.99	97.5	95	100
MLP	0.99	95	90	100

[c]using the Euclidean distance (ED), spectral angle mapper (SAM), logistic regression (Logi), support vector machine (SVM), and multilayer perceptron (MLP) with reference spectral signatures in the discrimination between seborrheic dermatitis and normal skin on the scalp (total number of patients = 40, number of patients with seborrheic dermatitis = 20, and number of normal subjects = 20). ROC-AUC, area under the receiver-operating characteristic curve

4. Discussion

In this study, we demonstrated the potentials of mobile multispectral imaging and analysis for discriminating between seborrheic dermatitis and psoriasis on the scalp. The developed system was capable of obtaining multispectral images within the wavelength range of 453 - 663 nm. The multispectral images were recorded using developed android applications. An image cube could be transferred to a server for discriminating between seborrheic dermatitis and psoriasis on the scalp, followed by the display of the resulting image on the smartphone. Moreover, it allowed self-monitoring of the diseased regions on the scalp through the smartphone. A previous report has shown that a smartphone-based multispectral imaging system has the potentials for diagnosing various skin lesions. However, the previous system showed some limitations in the examination of skin lesions [19]. For example, when the system was applied to examine skin lesions on the scalp, patients could not monitor the skin lesions of interest on a smartphone display. To address this limitation, an external CMOS

Biomedical Optics EXPRESS

camera was incorporated to the developed system for the self-diagnosis of skin lesions on the scalp rather than utilizing the camera in the smartphone. This enabled diseased regions on the scalp to be monitored in the smartphone display.

When the performance of the developed system was evaluated, a frequency line set at 45 cycles per millimeter could be clearly resolved in the vertical and horizontal directions by the system. In our previous study, the smartphone-based system was able to resolve a frequency line set at 51 cycles per millimeter [19]. The spatial resolution achieved by our proposed system was slightly lower than that by the previous system. It could be improved by utilizing a better external CMOS camera and a lens with a higher numerical aperture. Conversely, the system we developed herein also showed a slightly better performance than did the LCTF-based multispectral imaging system in multispectral imaging and analysis as shown in Fig. 4. The spectral classified images obtained using the LCTF showed more shot noise regions, more misclassified regions at the boundary of the letters, and lower contrast than did those obtained using our system. These might be because of the low signal-to-noise ratio in the detection of light owing to the low light transmission capability of the LCTF system.

In the discrimination between seborrheic dermatitis and psoriasis on the scalp using the system, the machine learning-based classification methods showed a relatively better performance than did the conventional spectral classification methods, particularly the SAM (Fig. 5). The spectral classified images of the psoriasis regions exhibited only a few misclassified regions, while most regions correctly indicated psoriasis. Therefore, via a simple quantification of the spectral classified images and appropriate threshold, such as calculating the ratio of the number of psoriasis and seborrheic dermatitis pixels, we could determine whether the skin lesions were psoriasis. Also, in the classified images for the seborrheic dermatitis [Fig. 5(a), bottom], we could still distinguish and classify the diseased regions as seborrheic dermatitis. The images of the patients with seborrheic dermatitis and psoriasis were obtained at a quite early stage; thus, it was challenging to classify between them even by an experienced clinician. Thus, these results suggest that the smartphone-based multispectral imaging and analysis may have a potential use for discriminating between seborrheic dermatitis and psoriasis in mobile environments.

For spectral classification, the ED, SAM, SVM, Logi, and MLP classification models were adopted. The machine learning models have previously been successfully utilized for detecting various diseases, including ovarian cancer [24], colonic and gastric cancers [25], prostate cancer [26], and Alzheimer's disease [27]. In previous studies, the machine learning models yielded strong classification outcomes for the detection of diseases. As in a previous study, three of the machine learning models constructed via multispectral imaging herein showed acceptable classification performance. The SVM model achieved the highest accuracy in the discrimination between them; it also had a better ROC-AUC (0.76) than the multilayered perceptron model (Table 1). In the comparisons between the three machine learning-based models and two conventional classification models, the sensitivities of the former were higher than those of the latter. The ROC-AUCs achieved by the machine learning models were also higher than those by the conventional classification models (Table 1). These results suggest that the machine learning-based models may provide better sensitivity and specificity compared with the conventional classification models; however, further clinical studies with larger numbers of patients are needed to confirm this.

In this study, to validate the performance of the constructed model under such conditions, 10-fold cross validation was performed owing to the relatively small number of patients with seborrheic dermatitis and psoriasis. This method has been typically utilized to evaluate the generalization and reproducibility of the machine learning-based models statistically. The specificity and sensitivity of the constructed models for discriminating between seborrheic dermatitis and psoriasis on the scalp were considerably high. Therefore, these results and consistent trends may provide confidence in the ability of multispectral imaging and analysis

Biomedical Optics EXPRESS

in discriminating between seborrheic dermatitis and psoriasis on the scalp based on the proposed models.

5. Conclusions

In conclusion, we employed multispectral imaging and analysis for discriminating between seborrheic dermatitis and psoriasis on the scalp using the smartphone-based multispectral imaging system we developed on the basis of various classification models, such as the ED, SAM, SVM, Logi, and MLP. The developed system was capable of performing multispectral imaging and analysis of lesions on the scalp for self-monitoring via a smartphone display. Herein, the machine learning methods (Logi, SVM, and MLP) for spectral classification showed a sensitivity of 65, 75, and 75 and specificity of 80, 70, and 70, respectively. The conventional methods (ED and SAM) showed a sensitivity of 70 and 70 and specificity of 70 and 75, respectively. Herein, the machine learning-based models yielded better outcomes than did the conventional methods, demonstrating the potential as a mobile detection device. Taken together, these results suggest that the multispectral imaging and analysis based on the machine learning techniques using the developed system would be a valuable tool for clinical diagnosis nearly in any setting; however, extensive clinical trials with a large number of patients are needed to confirm this.

Funding

National Research Foundation of Korea (NRF) (2014M3A9D707066, 2017M3A9G8084463).

Acknowledgments

Subjects recruitment was supported by Ohsang Kwon, M.D., Ph.D. Correspondence and requests for materials should be addressed to Dong Hun Lee, MD, PhD or Jae Youn Hwang, PhD.

Disclosures

The authors declare that there are no conflicts of interest related to this article.

References

1. A. K. Gupta, R. Bluhm, E. A. Cooper, R. C. Summerbell, and R. Batra, "Seborrheic dermatitis," Dermatol. Clin. **21**(3), 401–412 (2003).
2. T. Henseler and E. Christophers, "Psoriasis of early and late onset: characterization of two types of psoriasis vulgaris," J. Am. Acad. Dermatol. **13**(3), 450–456 (1985).
3. D. Jaliman, "Understanding Psoriasis–the Basics" (2015), retrieved 2015.
4. W.-H. Boehncke and M. P. Schön, "Psoriasis," Lancet **386**(9997), 983–994 (2015).
5. P. C. van de Kerkhof and M. E. Franssen, "Psoriasis of the scalp. Diagnosis and management," Am. J. Clin. Dermatol. **2**(3), 159–165 (2001).
6. G. W. Kim, H. J. Jung, H. C. Ko, M. B. Kim, W. J. Lee, S. J. Lee, D. W. Kim, and B. S. J. B. J. D. Kim, "Dermoscopy can be useful in differentiating scalp psoriasis from seborrhoeic dermatitis," Br. J. Dermatol. **164**(3), 652–656 (2011).
7. J.-H. Park, Y. J. Park, S. K. Kim, J. E. Kwon, H. Y. Kang, E.-S. Lee, J. H. Choi, and Y. C. Kim, "Histopathological differential diagnosis of psoriasis and seborrheic dermatitis of the scalp," Ann. Dermatol. **28**(4), 427–432 (2016).
8. P. Rosina, M. R. Zamperetti, A. Giovannini, and G. Girolomoni, "Videocapillaroscopy in the differential diagnosis between psoriasis and seborrheic dermatitis of the scalp," Dermatology (Basel) **214**(1), 21–24 (2007).
9. M. Kibar, Ş. Aktan, and M. Bilgin, "Dermoscopic findings in scalp psoriasis and seborrheic dermatitis; two new signs; signet ring vessel and hidden hair," Indian J. Dermatol. **60**(1), 41–45 (2015).
10. H. M. Subhash, "Biophotonics Modalities for High-Resolution Imaging of Microcirculatory Tissue Beds Using Endogenous Contrast: A Review on Present Scenario and Prospects," Int. J. Opt. **2011**, 20 (2011).
11. D. L. Farkas, G. Baxter, R. L. DeBiasio, A. Gough, M. A. Nederlof, D. Pane, J. Pane, D. R. Patek, K. W. Ryan, and D. L. Taylor, "Multimode light microscopy and the dynamics of molecules, cells, and tissues," Annu. Rev. Physiol. **55**(1), 785–817 (1993).
12. G. Kaminska-Winciorek and R. Spiewak, "Tips and tricks in the dermoscopy of pigmented lesions," BMC Dermatol. **12**(1), 14 (2012).

Biomedical Optics EXPRESS

13. T. Vo-Dinh, B. Cullum, and P. Kasili, "Development of a multi-spectral imaging system for medical applications," J. Phys. D Appl. Phys. **36**(14), 1663–1668 (2003).
14. Q. Li, X. He, Y. Wang, H. Liu, D. Xu, and F. Guo, "Review of spectral imaging technology in biomedical engineering: achievements and challenges," J. Biomed. Opt. **18**(10), 100901 (2013).
15. Y. Jung, J. Kim, O. Awofeso, H. Kim, F. Regnier, and E. Bae, "Smartphone-based colorimetric analysis for detection of saliva alcohol concentration," Appl. Opt. **54**(31), 9183–9189 (2015).
16. H. Kim, O. Awofeso, S. Choi, Y. Jung, and E. Bae, "Colorimetric analysis of saliva- alcohol test strips by smartphone-based instruments using machine-learning algorithms," Appl. Opt. **56**(1), 84–92 (2017).
17. M. Kim, S. Kim, M. Hwang, J. Kim, M. Je, J. E. Jang, D. H. Lee, and J. Y. Hwang, "Multispectral imaging based on a Smartphone with an external C-MOS camera for detection of seborrheic dermatitis on the scalp," in *SPIE BiOS*, (SPIE, 2017)
18. W. Groner, J. W. Winkelman, A. G. Harris, C. Ince, G. J. Bouma, K. Messmer, and R. G. Nadeau, "Orthogonal polarization spectral imaging: a new method for study of the microcirculation," Nat. Med. **5**(10), 1209–1212 (1999).
19. S. Kim, D. Cho, J. Kim, M. Kim, S. Youn, J. E. Jang, M. Je, D. H. Lee, B. Lee, D. L. Farkas, and J. Y. Hwang, "Smartphone-based multispectral imaging: system development and potential for mobile skin diagnosis," Biomed. Opt. Express **7**(12), 5294–5307 (2016).
20. J. Han, J. Pei, and M. Kamber, *Data mining: concepts and techniques* (Elsevier, 2011).
21. C.-I. Chang, *Hyperspectral imaging: techniques for spectral detection and classification* (Springer Science & Business Media, 2003), Vol. 1.
22. A. Thakur and D. Mishra, "Hyper spectral image classification using multilayer perceptron neural network & functional link ANN," in *Cloud Computing, Data Science & Engineering-Confluence, 2017 7th International Conference on*, (IEEE, 2017), 639–642.
23. F. Pedregosa, G. Varoquaux, A. Gramfort, V. Michel, B. Thirion, O. Grisel, M. Blondel, P. Prettenhofer, R. Weiss, and V. Dubourg, "Scikit-learn: Machine learning in Python," J. Mach. Learn. Res. **12**, 2825–2830 (2011).
24. T. H. Tate, B. Baggett, P. F. Rice, J. W. Koevary, G. V. Orsinger, A. C. Nymeyer, W. A. Welge, K. Saboda, D. J. Roe, K. D. Hatch, S. K. Chambers, U. Utzinger, and J. K. Barton, "Multispectral fluorescence imaging of human ovarian and fallopian tube tissue for early-stage cancer detection," J. Biomed. Opt. **21**(5), 056005 (2016).
25. D. Pantalone, F. Andreoli, F. Fusi, V. Basile, G. Romano, G. Giustozzi, L. Rigacci, R. Alterini, M. J. C. G. Monici, and Hepatology, "Multispectral imaging autofluorescence microscopy in colonic and gastric cancer metastatic lymph nodes," **5**, 230–236 (2007).
26. Y. Artan, M. A. Haider, D. L. Langer, T. H. van der Kwast, A. J. Evans, Y. Yang, M. N. Wernick, J. Trachtenberg, and I. S. Yetik, "Prostate cancer localization with multispectral MRI using cost-sensitive support vector machines and conditional random fields," IEEE Trans. Image Process. **19**(9), 2444–2455 (2010).
27. W. P. dos Santos, R. E. de Souza, and P. B. dos Santos Filho, "Evaluation of Alzheimer's disease by analysis of MR images using multilayer perceptrons and Kohonen SOM classifiers as an alternative to the ADC maps," in *Engineering in Medicine and Biology Society, 2007. EMBS 2007. 29th Annual International Conference of the IEEE*, (IEEE, 2007), 2118–2121.